

THE OBSERVABLE EFFECTS OF A PHOTOSPHERIC COMPONENT ON GRB'S AND XRF'S PROMPT EMISSION SPECTRUM

ASAF PE'ER^{1,2}, PETER MÉSZÁROS² AND MARTIN J. REES³

Draft version May 6, 2019

ABSTRACT

A thermal radiative component is likely to accompany the first stages of the prompt emission of Gamma-ray bursts (GRB's) and X-ray flashes (XRF's). We analyze the effect of such a component on the observable spectrum, assuming that the observable effects are due to a dissipation process occurring below or near the thermal photosphere. We consider both the internal shock model and a 'slow heating' model as possible dissipation mechanisms. For comparable energy densities in the thermal and the leptonic component, the dominant emission mechanism is Compton scattering. This leads to a nearly flat energy spectrum ($\nu F_\nu \propto \nu^0$) above the thermal peak at $\approx 10 - 100$ keV and below $10 - 100$ MeV, for a wide range of optical depths $0.03 \lesssim \tau_{\gamma e} \lesssim 100$, regardless of the details of the dissipation mechanism or the strength of the magnetic field. At lower energies steep slopes are expected, while above 100 MeV the spectrum depends on the details of the dissipation process. For higher values of the optical depth, a Wien peak is formed at $100 \text{ keV} - 1 \text{ MeV}$, and no higher energy component exists. For any value of $\tau_{\gamma e}$, the number of pairs produced does not exceed the baryon related electrons by a factor larger than a few. We conclude that dissipation near the thermal photosphere can naturally explain both the steep slopes observed at low energies and a flat spectrum above 10 keV, thus providing an alternative scenario to the optically thin synchrotron - SSC model.

Subject headings: gamma rays: bursts — gamma rays: theory — plasmas — radiation mechanisms: non-thermal

1. INTRODUCTION

The prompt emission from gamma-ray bursts (GRB's) is believed to arise from the prompt dissipation of a substantial fraction of the bulk kinetic energy of a relativistic outflow, originating from a central compact object (for reviews, see Mészáros 2002; Waxman 2003; Piran 2004). The dissipated energy is converted to energetic electrons, which produce high energy photons by synchrotron radiation and inverse Compton (IC) scattering. This model was found consistent with a large number of GRB observations (Band *et al.* 1993; Tavani 1996; Preece *et al.* 1998b). However, motivated by an increasing evidence for low energy spectral slopes steeper than the optically-thin synchrotron or synchrotron self Compton (SSC) model predictions (Crider *et al.* 1997; Preece *et al.* 1998b; Frontera *et al.* 2000; Ghirlanda, Celloti & Ghisellini 2003), an additional thermal component was suggested which may contribute to the observed spectrum (Mészáros & Rees 2000; Mészáros, Ramirez-Ruiz, Rees & Zhang 2002; Rees & Mészáros 2005). Indeed, thermal radiation originating from the base of the relativistic flow where the densities are high enough to provide (at least approximate) thermal equilibrium is an inevitable ingredient. This radiation is advected outward as long as the flow (presumably, jetted) material remains opaque, and eventually emerges highly collimated once the flow becomes optically thin, at distance r_{ph} from the core, which defines the photospheric radius. The comoving

energy density of this thermal radiation is comparable to the energy density of the relativistic outflow, in the first stages of the flow.

The rapid variability observed in GRB's, if interpreted in the framework of the internal collisions model, implies that (at least some of) the internal collisions occur at radii smaller than the photosphere radius (Mészáros & Rees 2000; Rees & Mészáros 2005). A similar conclusion can be drawn if alternative energy dissipation mechanisms are considered, such as magnetic reconnection (Thompson 1994; Giannios & Spruit 2005). If the energy dissipation occurs below or near the photospheric radius, the thermal photons serve as seed photons to IC scattering by the relativistic electrons. For high optical depth to scattering by the electrons (and the created pairs), the optically thin synchrotron-SSC model predictions are not valid, and a different analysis is needed.

Saturated Comptonization of (synchrotron) soft photons was studied in the past in the context of X-rays emission from X-ray bursters (Sunyaev & Titarchuk 1980; Pozdniakov *et al.* 1983; Zdziarski 1986; Zdziarski *et al.* 1994). It was first suggested as a source of GRB prompt emission by Liang, Kusunose, Smith & Crider (1997), and Liang (1997). Comptonization by thermal population of electrons was considered by Ghisellini & Celloti (1999) as an alternative source for GRB prompt emission. This model differs from the common "internal shock" model in that it assumes that the dissipated kinetic energy is continuously distributed among all the shell electrons, rather than being deposited into a small fraction of electrons that pass through the shock wave, and it assumes that the energy is equally distributed among electrons rather than following a power law distribution.

¹ Astronomical institute "Anton Pannekoek", Kruislaan 403, 1098SJ Amsterdam, the Netherlands; apeer@science.uva.nl

² Department of Astronomy and Astrophysics, Pennsylvania state university, University Park, PA 16802

³ Institute of Astronomy, university of Cambridge, Madingley Rd., Cambridge CB3 0HA, UK

The implication of these models were further analyzed by Pe'er & Waxman (2004) (see also Ramirez-Ruiz 2005).

In a previous paper (Pe'er, Mészáros & Rees 2005) we showed that clustering of the peak energy at 100 keV – 1 MeV as observed in many GRB's (Brainerd 1998; Preece *et al.* 1998a) can be naturally explained as being due to a Compton- inverse Compton scattering balance, if the kinetic energy dissipation process occurs below the Thompson photosphere. This result was found to be independent on the nature of the dissipation process.

In this paper, we analyze in greater depth the effect of a photospheric term on the prompt emission from GRB's and XRF's, under different assumptions about the unknown values of the free parameters of the emission models. In §2 we show that the energy carried by the thermal photons is comparable to the dissipated energy for plausible values of the free parameters characterizing GRB's. This implies a large radiative efficiency, in contrast to conventional internal shock models. We analyze in §3 the spectra obtained in the 'slow heating' scenario, and in §4 the spectra obtained in the 'internal shock' scenario. We show that these two different scenarios lead to very similar spectra for a large range of parameters values. In particular, we show here that a flat energy per decade spectrum $\nu F_\nu \propto \nu^0$ arises naturally above a thermal peak at 30-100 keV. This provides a natural explanation for the ubiquitous $F_\nu \propto \nu^{-1}$ prompt emission spectra (Band *et al.* 1993; Preece *et al.* 2000) in the sub-MeV to MeV range. At lower energies, the spectrum depends on the details of the scenario considered; it is generally steeper than the typical synchrotron spectrum, and can become flatter through superposition of different regions. In §5 we present numerical results, which confirm the validity of the analytical calculations in §3, §4, and provide further details of the spectra under various conditions. We discuss in §6 the implications of the possibility presented here of explaining the prompt emission by a scenario influenced by a photospheric component, different from the "standard" optically thin synchrotron-SSC model, as well as the applicability of this model to other compact objects, such as blazars.

2. ENERGY DISSIPATION AND THERMAL COMPONENT

Following the analysis of Rees & Mészáros (2005), we assume that the photospheric radius r_{ph} , which is defined as the radius above which the comoving optical depth along the jet falls to unity, lies outside the saturation radius r_s , at which the bulk Lorentz factor of the relativistic flow Γ asymptotes to the dimensionless entropy $\eta = L_0/(\dot{M}c^2)$, where L_0 and \dot{M} are the total energy and mass outflow rates. The saturation radius is $r_s \sim r_0\eta$, where r_0 is the radius at the base of the flow (where the energy is released), which is comparable to the Schwarzschild radius r_g of a central object of mass M , $r_0 \sim \alpha r_g = \alpha 2GM/c^2$ where $\alpha \geq 1$. Inside the saturation radius, the observer-frame photospheric luminosity L_γ is approximately the total luminosity of the outflow L_0 , since the increasing Doppler boost cancels the adiabatic decay of the comoving characteristic photon energy. At larger radius, $r > r_s$, the Lorentz factor no longer grows, and $L_\gamma(r) = L_0(r/r_s)^{-2/3} < L_0$, the greater part of the energy being in kinetic form, $L_k \sim L_0$.

We assume the existence of a dissipation pro-

cess, such as magnetic reconnection (Thompson 1994; Giannios & Spruit 2005) or internal shock waves within the expanding wind (Rees & Mészáros 1994; Woods & Loeb 1995; Sari & Piran 1997) that dissipates a fraction ϵ_d of the kinetic energy. As a concrete example for a dissipation process, we chose the internal shock model of GRB's, in which variation of the flow $\Delta\Gamma \sim \Gamma$ on a time scale $\Delta t \sim r_0/c$ results in the development of shocks at radius $r_i \approx 2\Gamma r_s$. At this radius, the photospheric luminosity is $L_\gamma(r_i) = L_0(2\Gamma)^{-2/3}$, and the comoving normalized temperature of the thermal component is

$$\theta \equiv \frac{k_B T'}{m_e c^2} = \frac{k_B}{m_e c^2} \left(\frac{L_0}{4\pi r_i^2 \Gamma^2 c a} \right)^{1/4} (2\Gamma)^{-2/3} \quad (1)$$

$$= 1.2 \times 10^{-3} L_{52}^{1/4} \Gamma_2^{-5/3} (\alpha m_1)^{-1/2},$$

where k_B , a are Boltzmann's and Stefan's constants, $L_0 = 10^{52} L_{52} \text{erg s}^{-1}$, $\Gamma = 10^2 \Gamma_2$, and the characteristic mass $M \sim 10 m_1$ solar masses of the central object (e.g. black hole) assumed, resulting in Schwarzschild radius $r_g = 2GM/c^2 \simeq 3 \times 10^6 m_1 \text{ cm}$.

The comoving proton number density in the shocked plasma at r_i is $n_p \approx L_0/(4\pi r_i^2 c \Gamma^2 m_p c^2)$, therefore the optical depth to Thompson scattering by the baryon related electrons at this radius is

$$\tau_{\gamma e} = \Gamma r_0 n_p \sigma_T = 100 L_{52} \Gamma_2^{-5} \alpha^{-1}. \quad (2)$$

We thus find that for the parameters values that characterizes GRB's, indeed $r_i < r_{ph}$.

We assume that a fraction ϵ_d of the kinetic energy is dissipated by the dissipation process, resulting in an internal energy density $u_{int} = L_0 \epsilon_d / 4\pi r_i^2 c \Gamma^2$. Fractions ϵ_e and ϵ_B of this energy are carried by the electrons and the magnetic field, respectively, therefore the ratio of the thermal photon energy density $u_{ph} = aT'^4$ to the electron energy density is

$$A \equiv \frac{u_{ph}}{u_{el}} = 0.44 \Gamma_2^{-2/3} \epsilon_{d,-1}^{-1} \epsilon_{e,-0.5}^{-1}, \quad (3)$$

where $\epsilon_d = 10^{-1} \epsilon_{d,-1}$, $\epsilon_e = 10^{-0.5} \epsilon_{e,-0.5}$ and $u_{el} \equiv \epsilon_e u_{int}$. Since the thermal photons provide the main photon reservoir for electron scattering, the ratio of synchrotron and IC emitted power by the electrons is

$$S \equiv \frac{P_{syn}}{P_{IC}} = \frac{u_B}{u_{ph}} = 1.1 \Gamma_2^{2/3} \epsilon_{d,-1} \epsilon_{B,-0.5}, \quad (4)$$

where $\epsilon_B = 10^{-0.5} \epsilon_{B,-0.5}$, and $u_B \equiv \epsilon_B u_{int}$.

In order to determine the resulting spectrum, the particle energy distribution needs to be specified. In the analysis below, we consider two alternative scenarios: the "slow heating" scenario, and the more widely used internal shock scenario, in which power-law energy distribution of the injected electrons is assumed.

3. SLOW HEATING SCENARIO

In this scenario, as suggested by Ghisellini & Celloti (1999), the dissipated energy is continuously and evenly distributed among the shell's electrons, during the comoving dynamical time of the dissipation process, $t_{dyn} \equiv \Gamma \Delta t$. The electrons are assumed to have a Maxwellian distribution with normalized temperature θ_{el} , and Comptonization is the main emission mechanism.

The electron temperature is determined by energy balance between the energy injection rate, $dE_+/dt = u_{el}/n_{el}t_{dyn}$, and energy loss rate. For optical depth $\tau_{\gamma e}$ not much larger than unity, the energy loss rate is given by $dE_-/dt = (4/3)c\sigma_T(\gamma_f\beta_f)^2u_{ph}(1+S)$. Here, n_{el} is the number density of electrons in the plasma, $n_{el} = n_p$, pairs are neglected (see below), and $\gamma_f\beta_f$ is the electron momentum, which for a relativistic Maxwell-Boltzmann distribution is related to the temperature via $\theta_{el} = \gamma_f\beta_f^2/(1+\beta_f^2)$. At steady state, the electron momentum is therefore given by

$$\gamma_f\beta_f = \left(\frac{3}{4}\frac{1}{\tau_{\gamma e}A(1+S)}\right)^{1/2}. \quad (5)$$

Since A and $(1+S)$ are of order unity for parameters characterizing GRB's, $\gamma_f\beta_f \simeq \tau_{\gamma e}^{-1/2}$.

The resulting spectrum above the thermal peak can now be approximated in the following way. For $\gamma_f\beta_f \gtrsim 1$ ($\tau_{\gamma e} \lesssim 1$), the energy of a photon after n_{sc} scattering is $\varepsilon_{n_{sc}} \approx (\gamma_f\beta_f)^{2n_{sc}}\varepsilon_0$, where ε_0 is the initial photons' energy. In the Thompson regime, the scattering rate is $dn_{ph}/dt \approx n_{ph,0}n_{el}c\sigma_T = n_{ph,0}\tau_{\gamma e}/t_{dyn}$, where $n_{ph,0}$ is the number density of photons at the thermal peak. At the end of the dynamical time, the number density of photons that undergo n_{sc} scattering is therefore $n_{ph,n_{sc}} \approx n_{ph,0}\tau_{\gamma e}^{n_{sc}}$. These photons have energies in the range $\varepsilon_{n_{sc}} \dots \varepsilon_{n_{sc}} + d\varepsilon_{n_{sc}}$, therefore

$$\begin{aligned} \log\left(\frac{n_{ph,n_{sc}}}{n_{ph,0}}\right) &= \log\left(\frac{\varepsilon_{n_{sc}}}{\varepsilon_0}\right) \times \frac{\log \tau_{\gamma e}}{\log(\gamma_f\beta_f)^2} \\ &= \log\left(\frac{\varepsilon_{n_{sc}}}{\varepsilon_0}\right) \times (-1), \end{aligned} \quad (6)$$

where A not much different than 1 and S not much larger than 1 assumed in the last equality, resulting in $(\gamma_f\beta_f)^2 \approx \tau_{\gamma e}^{-1}$. Since $n_{ph,n_{sc}}$ is the number density of photons in the range $\varepsilon_{n_{sc}} \dots \varepsilon_{n_{sc}} + d\varepsilon_{n_{sc}}$, we conclude that $\varepsilon_{dn}/d\varepsilon \propto \varepsilon^{-1}$, or $\nu F_\nu \propto \nu^0$ above the thermal peak and below $\varepsilon_{max} = \gamma_f m_e c^2$ (in the plasma frame).

For $\tau_{\gamma e} \ll 1$, the electron momenta at steady state $\gamma_f\beta_f \gg 1$. An upper limit on the electron momenta $\gamma_f\beta_f \sim \gamma_f$ is $\gamma_f \leq \tilde{\gamma} \equiv u_{el}/n_{el}m_e c^2 = (m_p/m_e)\epsilon_d \epsilon_e \gamma_p = 60\epsilon_{d,-1}\epsilon_{e,-0.5}\gamma_{p,0}$, where $(\gamma_p - 1)m_p c^2$ is the proton's thermal energy and $\gamma_p = 1\gamma_{p,0}$ (cold protons) assumed. This value is achieved if the optical depth is $\tau_{\gamma e} \leq \hat{\tau}_{\gamma e} \approx 3 \times 10^{-4} A_0^{-1} \epsilon_{d,-1}^{-2} \epsilon_{e,-0.5}^{-2} \gamma_{p,0}^{-2}$ where $A = 1A_0$, and equation 5 was used. For lower value of $\tau_{\gamma e}$, the photons receive only a small fraction of the electron's energy. In this case only 1-2 scatterings are required to upscatter photons to $\varepsilon_{max} = \gamma_f m_e c^2$. We therefore expect a spectrum with a wavy shape, composed of a low energy synchrotron peak, thermal peak, and few IC peaks (see the numerical results in §5 below).

For high value of the optical depth, $\tau_{\gamma e}$ larger than a few, the electrons momenta satisfy $\gamma_f\beta_f < 1$. If the optical depth is high enough, the photons receive nearly all of the electrons energy, and a Wien peak is formed at

$$\varepsilon_{WP} \approx 3\theta m_e c^2 \times \left(1 + \frac{1}{A}\right) \approx 6 \text{ keV} \quad (7)$$

(in the plasma frame), where equations 1, 3 were used. Electrons up-scatter photons up to energy $(\gamma_f\beta_f)^2 m_e c^2$, therefore equation 7 sets a lower limit on $\gamma_f\beta_f$, $\gamma_f\beta_f \gtrsim$

0.1. Equation 5 can now be used to find the value of $\tau_{\gamma e}$ above which the Wien peak is formed, $\tau_{\gamma e} > \tilde{\tau}_{\gamma e} \approx (3/4)(100/A(1+S)) \approx 80A_0^{-1}$. We thus conclude that for optical depth larger than ~ 100 , the spectrum approaches a Wien spectrum, and equation 7 provides an asymptotic limit of the Wien peak energy. For $\tau_{\gamma e}$ of a few tens, the spectral slope below the Wien peak is softer than the Wien spectrum, $\nu F_\nu \propto \nu^\alpha$ with $\alpha \lesssim 3$. As a result the Wien peak is produced at energy somewhat higher than the asymptotic value given in equation 7.

For values of A not much smaller than 1, equation 5 implies that a large number of pairs cannot be produced. If $\tau_{\gamma e}$ is larger than unity, $\gamma_f\beta_f < 1$, the maximum energy of the up-scattered photons is smaller than $m_e c^2$, and no pairs are produced (for synchrotron emitted photons to be above $m_e c^2$, a magnetic field $B \gtrsim 10^{13}$ G is required). For $\tau_{\gamma e}$ smaller than 1, an upper limit on the number of the produced pairs can be obtained in the following way: For photon spectrum $I_\nu \propto \nu^{-1}$, assuming the upscattering photons receive all the electrons energy, the number density of photons energetic than $m_e c^2$ is approximated by $n_\gamma(\varepsilon > m_e c^2) \approx u_{el}/m_e c^2 \log(\gamma_f/3\theta)$. The rate of pair production is $dn_\pm/dt \approx (3/16)c\sigma_T n_\gamma(\varepsilon > m_e c^2) n_\gamma(m_e c^2/\gamma_f \lesssim \varepsilon \lesssim m_e c^2)$, where $n_\gamma(m_e c^2/\gamma_f \lesssim \varepsilon \lesssim m_e c^2)$ is the number density of photons that produce pairs with the energetic photons, $n_\gamma(m_e c^2/\gamma_f \lesssim \varepsilon \lesssim m_e c^2) \approx \gamma_f n_\gamma(\varepsilon > m_e c^2)$ for $I_\nu \propto \nu^{-1}$. The number density of the produced pairs at the end of the dynamical time is therefore $n_\pm \approx (3/16)c\sigma_T t_{dyn} \gamma_f u_{el}^2 / (m_e c^2 \log(\gamma_f/3\theta))^2$, or

$$\frac{n_\pm}{n_{el}} = \frac{3\tilde{\gamma}^2 \gamma_f \tau_{\gamma e}}{16 \log\left(\frac{\gamma_f}{3\theta}\right)^2} \sim 6\tau_{\gamma e}^{1/2}, \quad (8)$$

where characteristic value $\log(\gamma_f/3\theta) \approx 10$ assumed. For $\tau_{\gamma e}$ smaller than unity this result implies that pairs cannot outnumber the baryon related electrons by a factor larger than a few at most. For $\gamma_f \leq \tilde{\gamma} = 60$, a magnetic field larger than $\sim 10^{10}$ G is required for synchrotron emission at energies higher than $m_e c^2$, thus we conclude that pairs are not produced by synchrotron photons in this case of small $\tau_{\gamma e}$ as well.

4. INTERNAL COLLISION SCENARIO

We further explore the effect of a photospheric component on the observed spectrum in the more conventional internal shocks scenario, in which the dissipated energy is converted to acceleration of electrons to high energies. We assume a fraction $\epsilon_{pl} \leq 1$ of the electron number density n_{el} is accelerated to a power law energy distribution with power law index p in the range γ_{char} to γ_{max} . A fraction $1 - \epsilon_{pl}$ of the electrons are assumed to have a Maxwellian distribution with normalized temperature $\theta_{el} = \gamma_{char}/2$. Thermal photons are in the Klein-Nishina limit for Compton scattering by energetic electrons, therefore γ_{max} is determined by equating the acceleration time and the synchrotron loss time,

$$\gamma_{max} = 2.3 \times 10^4 \mathbf{L}^{-1/4} \epsilon_{d,-1}^{-1/4} \epsilon_{B,-0.5}^{-1/4} \Gamma_2^{3/2} \alpha_0^{1/2}, \quad (9)$$

where $\alpha = 1\alpha_0$. The characteristic Lorentz factor of the accelerated electrons is

$$\begin{aligned} \gamma_{char} &= \frac{\epsilon_e \epsilon_d \gamma_p \left(\frac{m_p}{m_e}\right)}{3/2(1-\epsilon_{pl}) + \epsilon_{pl} \log\left(\frac{\gamma_{max}}{\gamma_{char}}\right)} \\ &\simeq 30\epsilon_{e,-0.5}\epsilon_{d,-1}\gamma_{p,0}, \end{aligned} \quad (10)$$

where $\epsilon_{pl} = 0.1$ was taken, $\log(\gamma_{\max}/\gamma_{char}) \approx 7$ and a power law index $p = 2$ of the accelerated electrons above γ_{char} is assumed. Electrons having Lorentz factor γ lose their energy by Compton scattering and synchrotron emission on time scale $t_{loss} = \gamma m_e c^2 / (4/3) c \sigma_T \gamma^2 u_{ph} (1 + S)$, and cool down to $\gamma_f \simeq 1$ on time $t_{loss} = \tilde{t}_{loss} \times \gamma$. The ratio of the cooling time of electrons at γ_{char} to the dynamical time is calculated using equations 2,3, 4 and 10,

$$\frac{t_{loss}(\gamma_{char})}{t_{dyn}} = \frac{1}{(4/3)A(1+S)\gamma_{char}\tau_{\gamma e}} = \frac{0.03}{\tau_{\gamma e}} \Gamma_2^{2/3}. \quad (11)$$

We thus conclude that for Lorentz factor $\Gamma < 2 \times 10^4$, $\tau_{\gamma e} > 1$ directly implies $t_{loss}(\gamma_{char}) < t_{dyn}$, and electrons lose all their energy during the dynamical time.

If the optical depth to scattering is low, $\tau_{\gamma e} < 0.03 \Gamma_2^{2/3}$, electrons at γ_{char} maintain their energy during the dynamical time. The resulting inverse Compton spectrum in the range $\theta m_e c^2 \dots \gamma_{char}^2 \theta m_e c^2$ is $I_\nu \propto \nu$, or $\nu F_\nu \equiv \varepsilon^2 dn_\gamma / d\varepsilon \propto \varepsilon^2$. At higher energies, the spectral index is determined by the power law index of the injected electrons. Above $\gamma_{char} m_e c^2$ Klein Nishina effect significantly modifies the spectrum, and numerical treatment is required (see the numerical results in §5 below).

For an optical depth $0.03 \Gamma_2^{2/3} \lesssim \tau_{\gamma e} \lesssim 1$, electrons lose their energy and accumulate at $\gamma_f \sim 1$ at the end of the dynamical time. The energy loss rate of electrons at Lorentz factor $\gamma < \gamma_{char}$ is $p(\gamma) \propto \gamma^2 u_{ph} (1 + S) \propto \gamma^2$, therefore the electron distribution below γ_{char} is $n_{el}(\gamma) \propto \gamma^{-2}$, and the resulting IC spectrum in the range $\theta m_e c^2 \dots \gamma_{char} m_e c^2$ is $\nu F_\nu \equiv \varepsilon^2 dn_\gamma / d\varepsilon \propto \varepsilon^\alpha$ with $\alpha = 1/2$. On top of the IC component there is the synchrotron component from the power-law accelerated electrons, with spectral index $\alpha = 1 - p/2$. The observed spectral index in this range is therefore expected to be $\alpha \lesssim 0.5$, the exact value depends on the details of the scenario, i.e. the values of ϵ_{pl} , S and p . In §5 we present our numerical results in this case.

For higher optical depth, $\tau_{\gamma e} > 1$, electrons lose their energy by inverse Compton scattering and synchrotron emission, and accumulate at $\gamma_f \simeq 1$. At low energies, electrons are heated by direct Compton scattering energetic photons. We show in §A, that a photon with energy $\varepsilon > f m_e c^2$ where $f \approx 3$ interacting with low energy electrons having $\gamma \simeq 1$, lose energy at an energy-independent rate, $d\varepsilon/dt \simeq c \sigma_T n_{el} (m_e c^2 / 2)$. The injection rate of energetic photons (via IC scattering and synchrotron emission) is approximated using energy considerations, $dn_{ph}(\varepsilon > f m_e c^2) / dt \approx u_{el} / f m_e c^2 t_{dyn}$. These photons lose energy by downscattering to energies below $f m_e c^2$ on a time scale $\varepsilon / (d\varepsilon/dt) = 2 f t_{dyn} / \tau_{\gamma e}$, therefore at steady state the number density of energetic photons is given by $n_{ph}(\varepsilon \gtrsim f m_e c^2) \approx 2 u_{el} / m_e c^2 \tau_{\gamma e}$. This result implies that the energy gain rate of electrons via direct-Compton scattering is equal to the energy gain rate in the slow heating mechanism, $dE_+ / dt \simeq u_{el} / n_{el} t_{dyn}$ (see also Pe'er, Mészáros & Rees 2005), therefore for $\tau_{\gamma e}$ not much larger than unity, equation 5 characterizes the electron momenta at the end of the dynamical time in this scenario a well. We have previously shown (Pe'er, Mészáros & Rees 2005) that in this case of high optical depth, the electrons accumulate at $\gamma_f \beta_f \simeq 0.1$

with a very weak dependence on the values of the unknown parameters, and that for optical depth higher than a few tens a Wien peak is formed at 1 – 10 keV. Equation 7 provides the asymptotic value of the Wien peak energy for very high optical depth in this scenario as well. For $\tau_{\gamma e}$ of a few tens, the thermal peak is up-scattered to energy in the range $\theta m_e c^2 < \varepsilon_{peak} < \varepsilon_{WP}$ (see the numerical results in §5).

In contrast to the slow heating scenario, a large number of pairs can in principle be created, following the injection of particles to high energies. However, the following argument, based on the analysis of Pe'er & Waxman (2004) suggests that the number of pairs do not outnumber the baryon-related electrons by a factor larger than a few, for any value of the optical depth $\tau_{\gamma e}$. From energy considerations, the pair injection rate is limited by $dn_\pm / dt \approx u_{el} / m_e c^2 t_{dyn}$. The pair annihilation rate is $\sim n_\pm^2 c \sigma_T$, therefore the ratio of pairs to baryon-related electrons in steady state is

$$\frac{n_\pm}{n_{el}} \approx \left(\frac{\gamma_{char}}{\tau_{\gamma e}} \right)^{1/2}. \quad (12)$$

We therefore do not expect pairs to outnumber the baryon-related electrons by a number larger than a few for any value of the optical depth. The creation of pairs lowers the number density of energetic photons, thus lowering the value of $\gamma_f \beta_f$ by a small factor (see Pe'er, Mészáros & Rees 2005).

5. NUMERICAL CALCULATIONS

5.1. The numerical model

In order to confirm the analytical calculations presented above and to derive the spectra resulting from different values of the free parameters, we calculated numerically the photon and particle energy distribution under the assumptions of §3, §4. In our numerical calculations we used the time dependent numerical code presented in Pe'er & Waxman (2004b). This code solves self-consistently the kinetic equations for e^\pm and photons describing cyclo-synchrotron emission, synchrotron self absorption, direct and inverse Compton scattering, pair production and annihilation, and the evolution of a high energy electro-magnetic cascade. These equations are being solved during the dynamical time of the dissipation process.

In this version of the code, we assume the existence of a thermal photospheric component, which at the dissipation radius r_i is characterized by time independent luminosity $L_\gamma = L_0 (2\Gamma)^{-2/3}$ and temperature given by equation 1. A fraction $\epsilon_d = 0.1 \epsilon_{d,-1}$ of the kinetic energy is dissipated by the dissipation process. A fraction ϵ_e of the dissipated energy is carried by the electrons, and a fraction ϵ_B is carried by the magnetic field. In the slow heating scenario, the dissipated energy is assumed to be continuously distributed among the electrons in the two shells (and the created pairs), which assume a Maxwellian distribution with normalized temperature $\theta_{el}(t)$. The electron temperature is determined self-consistently at each time step by balance of energy injection and energy loss. In the internal shock scenario, electrons are assumed to be injected by the shock waves at a constant rate. A fraction ϵ_{pl} of the electron population is injected into a power-law energy distribution with

power-law index p between γ_{char} and γ_{max} (see eqs. 9, 10). The remaining fraction $1 - \epsilon_{pl}$ of the injected electrons assume a Maxwellian distribution with temperature $\theta_{el} = \gamma_{min}/2 \approx 20\epsilon_{e,-0.5}\epsilon_{d,-1}$.

5.2. Slow heating scenario

Numerical results of the observed spectra at the end of the dissipation process in the slow heating scenario are presented in Figure 1 for different values of the optical depth τ_{γ_e} . In producing the plots in this graph, we chose representative values of the free parameters, $\alpha = 1$, $\Gamma = 10^2$, $\epsilon_d = 10^{-1}$, $\epsilon_e = \epsilon_B = 10^{-0.5}$. The differences in the plots are due to different intrinsic luminosity, $L_0 = 10^{48} - 10^{53} \text{ erg s}^{-1}$ which result in a wide range of optical depths, $10^{-2} \leq \tau_{\gamma_e} \leq 10^3$ (see eq. 2). A similar graph is obtained by assuming different value of Γ and constant luminosity, where variation in the value of Γ by a factor of 3, leads to variation in τ_{γ_e} by a factor $10^{2.5}$.

In the case of low optical depth $\tau < 1$, one expects the thermal peak at the observed energy $3\theta\Gamma m_e c^2 / (1+z) \approx 10 - 100 \text{ keV}$, caused by the advected thermal photons. In the scenario of $\tau = 0.01$, the characteristic Lorentz factor of the electrons is $\gamma_f \approx 10$, and synchrotron radiation produces the peak observed at low energy, $\sim 300 \text{ eV}$. For higher optical depth the characteristic electron Lorentz factor is lower, $\gamma_f \gtrsim 1$ (see eq. 5), and the synchrotron emission occurs at lower energies, below the synchrotron self-absorption frequency (see the analysis of synchrotron self-absorption frequency as a function of the free parameters values in Pe'er & Waxman 2004).

The high value of the characteristic Lorentz factor of the electrons in the scenario with $\tau = 0.01$ implies that two scatterings are required to upscatter thermal photons to $\sim 100 \text{ MeV}$, therefore Compton scattering of the synchrotron and thermal photons produces the wavy shape of the spectrum above 10 keV .

At moderate values of the optical depth, $\tau \sim 0.1 - 10$, multiple Compton scattering produces the flat spectrum observed above the thermal peak, in the range $10 \text{ keV} - 10 \text{ MeV}$, in agreement with the predictions of §3. At even higher values of the optical depth, $\tau_{\gamma_e} \gtrsim 100$, a Wien peak is formed at sub MeV energy. As explained in Pe'er & Waxman (2004), the high optical depth implies that in this case photons are not observed prior to a period of adiabatic expansion, during which 50-70% of the photons' energy is converted to kinetic energy (bulk motion) of the plasma. The observed Wien peak is therefore expected at $\approx 300 \text{ keV}$ (see also Pe'er, Mészáros & Rees 2005).

5.3. Comparison of scenarios: low optical depth

Figure 2 shows comparison of the spectra obtained for the two dissipation scenarios considered (slow heating and internal shocks) and two different values of the magnetic field, in the scenario of very low optical depth, $\tau_{\gamma_e} = 4 \times 10^{-3}$. For this value of the optical depth, only a small fraction of the electrons energy is radiated. If the magnetic field is weak (dash-dotted lines), the advected thermal peak at 10 keV is prominent. In the slow heating scenario (thin dash-dotted line) an IC peak at $\sim 15 \text{ MeV}$, created by electrons having $\gamma_f \beta_f = 30$ is expected. The thin solid line, representing the slow heating scenario with equipartition magnetic field, shows four peaks: The synchrotron peak at 300 eV , the thermal peak at 10 keV

and two peaks produced by IC scattering the low energy peaks, at 300 keV and 10 MeV . The combined effect of these peaks is a wavy shaped, nearly flat spectrum in the range $100 \text{ eV} - 100 \text{ MeV}$.

An internal shock scenario with weak magnetic field is shown by the thick dash-dotted line in Figure 2. Electrons injected with a power law index $p = 2$ between γ_{char} and γ_{max} produce the high energy component by IC scattering the thermal photons. Electrons with Lorentz factor $\gamma < \bar{\gamma} = (4\theta)^{-1} = 3 \times 10^3$ cool by IC emission faster than the dynamical time, therefore the resulting IC spectrum is nearly flat, $\nu F_\nu \equiv \epsilon^2 dn_\gamma / d\epsilon \propto \epsilon^\alpha$ with $\alpha = 0$ below $\Gamma \bar{\gamma}^2 \theta m_e c^2 / (1+z) \simeq 30 \text{ GeV}$. For energetic electrons with $\gamma > \bar{\gamma}$, the thermal photons are in the Klein-Nishina regime, and as a result these electrons cool slower than the dynamical time, and the spectral slope of the IC spectrum at higher energies is $\alpha = 1/2$. If magnetic field is added (thick, solid curve), electrons at all energies cool fast by synchrotron emission, and the resulting synchrotron spectrum is flat in the range $100 \text{ eV} - 10 \text{ GeV}$.

5.4. Comparison of scenarios: intermediate and high optical depth

For low to moderate values of τ_{γ_e} , equation 5 provides a good estimate of the electron momenta. The ratio between the energy of the synchrotron peak ϵ_{syn} and the energy of the thermal peak $\epsilon_{th} = 3\theta m_e c^2$ is given by

$$\begin{aligned} \frac{\epsilon_{syn}}{\epsilon_{th}} &= \frac{3 \hbar q B (\gamma_f \beta_f)^2}{2 m_e c \epsilon_{th}} \\ &= \left(\frac{\pi a}{8} \right)^{1/2} \frac{2^{1/3}}{k_B^2} \frac{\hbar q}{m_e c} \frac{\Gamma^{1/3} (\epsilon_B \epsilon_d)^{1/2} \epsilon_{th}}{A(1+S)\tau_{\gamma_e}} \\ &= \frac{4.5 \times 10^{-4}}{\tau_{\gamma_e}} \Gamma_2^{1/3} \epsilon_{d,-1}^{1/2} \epsilon_{B,-0.5}^{1/2} A_0^{-1} \epsilon_{th,4}^{ob}, \quad (13) \end{aligned}$$

where $\epsilon_{th}^{ob} = 10^4 \epsilon_{th,4}^{ob} \text{ eV}$ is the observed energy of the thermal peak. We therefore conclude that for $\tau_{\gamma_e} \gtrsim 0.1$ the peak energy of the synchrotron component is much lower than the peak energy of the thermal component, and is below the self absorption frequency for $\tau_{\gamma_e} \gtrsim 1$. This conclusion is confirmed by the numerical results of the slow heating scenario (thin line) with strong (solid) magnetic field, presented in Figures 3 and 4 for $\tau_{\gamma_e} = 0.1, 1$ respectively. A low energy synchrotron component at $\sim 200 \text{ eV}$ is prominent for $\tau_{\gamma_e} = 0.1$ (Figure 3), and is much weaker for $\tau_{\gamma_e} = 1$ (Figure 4).

Figures 3-5 provide a comparison of the spectra obtained for the two dissipation mechanisms, equipartition vs. low magnetic field, and two different values of ϵ_{pl} . The internal shock scenario is shown with the thick lines in Figure 3. The solid line denote the scenario of equipartition magnetic field and $\epsilon_{pl} = 0$, i.e., the electrons are injected at γ_{char} and than cool to γ_f . Synchrotron emission dominates the spectrum below the thermal peak, at $0.1 - 10 \text{ keV}$, and IC scattering dominates at higher energies. The electron distribution below γ_{char} is $n_{el}(\gamma) \propto \gamma^{-2}$, therefore the emitted radiation has spectral slope $\alpha = 1/2$. IC scattering by electrons accumulated at γ_f results in somewhat flatter ($\alpha \lesssim 1/2$) spectral slope. The thick dash-dotted curve shows a scenario with weak magnetic field ($\epsilon_B = 10^{-6}$) and $\epsilon_{pl} = 1$. In this scenario, energetic electrons upscatter photons to

high energies; however, pair production suppresses emission above GeV. The number of pairs created in this scenario is found numerically to be $n_{\pm}/n_{el} \simeq 4$, in agreement with the analytical predictions of §4.

The numerical results obtained for $\tau_{\gamma e} = 1, 10$ are presented in Figures 4 and 5. These results further show the similarity between the spectra obtained by the two different dissipation mechanisms, as well as the weak dependence of the spectral shape on the value of the magnetic field or on ϵ_{pl} . Multiple scattering creates the flat energy per decade spectrum above the thermal peak at $3\theta\Gamma m_e c^2/(1+z) \simeq 30 - 100$ keV, for a typical $\Gamma = 100 - 300$. This energy is very similar, albeit somewhat lower than the observed spectral break energy, ~ 300 keV (Band *et al.* 1993; Preece *et al.* 1998a, 2000). The flat spectrum extends up to $\Gamma(\gamma_f \beta_f) m_e c^2/(1+z) \approx 10$ MeV.

In the internal shock scenario, the energetic photons produce pairs, resulting in a cutoff above ~ 100 MeV. The number density of pairs in the scenario $\tau_{\gamma e} = 1$ is found numerically to be $n_{\pm}/n_{el} \simeq 4$ ($\epsilon_{pl} = 0$), $n_{\pm}/n_{el} \simeq 5$ ($\epsilon_{pl} = 1$). Similar, but somewhat lower values ($n_{\pm}/n_{el} = 1.5, 3.5$, respectively) are obtained for $\tau_{\gamma e} = 10$. We thus find that, indeed, pairs do not outnumber the baryon related electrons by a large factor, due to pair annihilation. The pair annihilation phenomenon causes the small peak observed at $\Gamma m_e c^2/(1+z) = 25$ MeV (see Pe'er & Waxman 2004, for further discussion). In summary, for intermediate values of the optical depth $\tau_{\gamma e} \approx 0.1 - 10$, multiple IC scattering produces an approximately flat energy per decade spectrum in the range \approx keV - sub GeV for the two dissipation mechanism considered regardless of the values of the magnetic field or of ϵ_{pl} .

Figure 6 shows the asymptotic case of high optical depth, $\tau_{\gamma e} = 100, 1000$. For optical depth larger than ~ 100 , multiple Compton scattering leads to the formation of a Wien peak at sub- MeV energies, regardless of the details of the acceleration mechanism, or the values of any of the free parameters (see also Pe'er, Mészáros & Rees 2005). As shown in §4, for high values of the optical depth the number density of pairs is strongly suppressed by pair annihilation. This calculation is confirmed by the numerical results, $n_{\pm}/n_{el} \simeq 1$.

6. SUMMARY AND DISCUSSION

In this work, we have considered the effect of a photospheric component on the observed spectrum after kinetic energy dissipation that occurs below or near the thermal photosphere of the outflows in GRB's or XRF's, with particular emphasis on the resulting spectral shape. Two dissipation mechanisms were considered: the “slow heating” mechanism, and the internal shock scenario. We showed that the resulting spectra are largely independent on the details of the dissipation mechanism or of the values of any of the free parameters. A strong dependence was found only on the value of the optical depth, $\tau_{\gamma e}$. For $\tau_{\gamma e}$ smaller than a few tens, an approximately flat energy per decade spectrum is obtained above a break energy at few tens - hundred keV and up to sub GeV, while steep slopes are obtained below the break energy (see Figures 4, 5). For higher values of the optical depth, a Wien peak is formed at sub MeV energies, with steep slope at lower energies, and sharp cutoff above this energy. The production of pairs does not change this re-

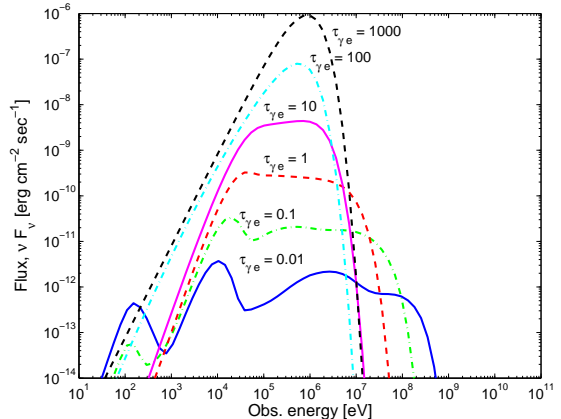


FIG. 1.— Time averaged spectra obtained for different values of optical depth, $\tau_{\gamma e}$ in the slow heating scenario. Results are for $\alpha = 1$, $\Gamma = 100, \epsilon_d = 0.1$, $\epsilon_e = 10^{-0.5}$ and GRB luminosity $L = 10^{-4}, 10^{-3}, 10^{-2}, 10^{-1}, 10^0, 10^1, 10^2$, with corresponding optical depth $\tau_{\gamma e} = 10^{-2} - 10^3$ (see eq. 2). $\epsilon_B = 10^{-0.5}$ for $L = 10^{-4} - 10^0$, and $\epsilon_B = 10^{-6}$ for $L = 10^1, 10^2$. A redshift $z = 1$ in a flat universe with $\Omega_m = 0.3$, $\Omega_\Lambda = 0.7$, $H_0 = 70$ is assumed. The spectrum is not corrected for the energy loss due to adiabatic expansion following the dissipation, which lowers the energy for the cases of $L = 10^1, 10^2$ ($\tau_{\gamma e} = 10^2, 10^3$) by a factor of 2-3.

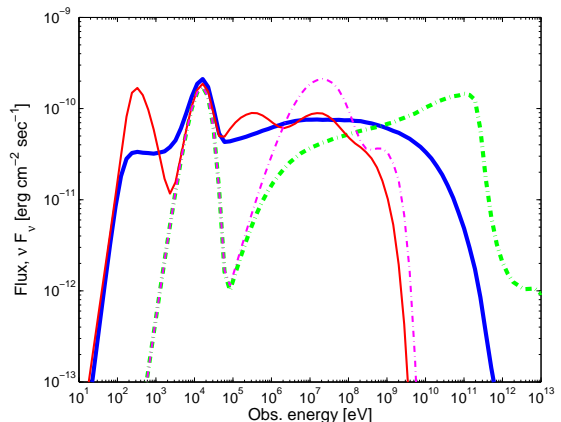


FIG. 2.— Time averaged spectra obtained for low value of the optical depth, $\tau_{\gamma e} = 4 \times 10^{-3}$. $\alpha = 1$, $L = 10^{-2}$, $\Gamma = 300$, $\epsilon_d = 0.1$, $\epsilon_e = 10^{-0.5}$ assumed. Results for slow dissipation are shown in thin lines and dissipation by shock waves with power law index $p = 2$ and $\epsilon_{pl} = 1$ are presented in thick lines. Solid lines are for high magnetic field, $\epsilon_B = 10^{-0.5}$ and dash-dotted lines are for $\epsilon_B = 10^{-6}$. $z = 1$ with the same cosmological parameters as in figure 1.

sult, since pair annihilation limits the ratio of the number density of pairs to baryon-related electrons to a factor not larger than a few.

Our theoretical and numerical results emphasize the important role of inverse Compton scattering in the formation of the spectra in scenarios involving an important thermal component. As a consequence, the observed spectral slopes in the two model considered are significantly different than the synchrotron model prediction. The (nearly) thermal component observed for low to intermediate values of the optical depth, and the Wien peak formed for high value of the optical depth can account for the increasing evidence for steep spectral slopes observed below ~ 100 keV in the early stages of GRB's (Preece *et al.* 2002;

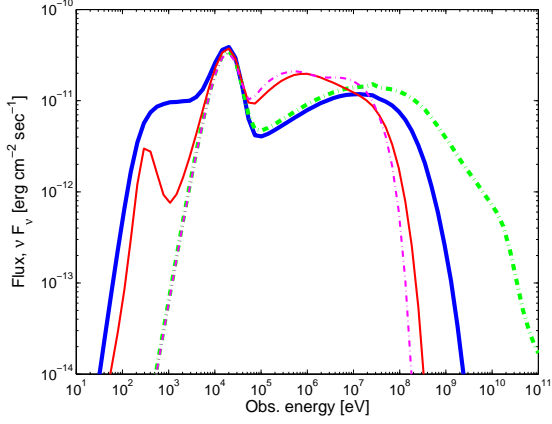


FIG. 3.— Time averaged spectra obtained for low value of the optical depth, $\tau_{\gamma e} = 0.1$. $\alpha = 1$, $L = 10^{-3}$, $\Gamma = 100$, $\epsilon_d = 0.1$, $\epsilon_e = 10^{-0.5}$ assumed. Results for slow dissipation are shown in thin lines and dissipation by shock waves with power law index $p = 2$ are presented in thick lines. Solid lines are for high magnetic field, $\epsilon_B = 10^{-0.5}$ and dash-dotted lines are for $\epsilon_B = 10^{-6}$. $\epsilon_{pl} = 0$ (thick, solid), and $\epsilon_{pl} = 1$ (thick, dash-dotted). $z = 1$ with the same cosmological parameters as in figure 1.

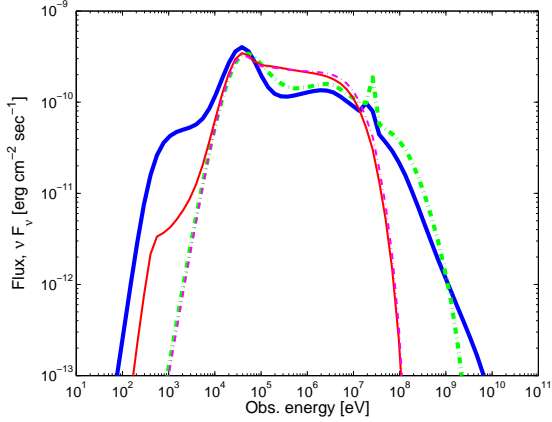


FIG. 4.— Time averaged spectra obtained for low value of the optical depth, $\tau_{\gamma e} = 1$. Results are shown for $L = 10^{-2}$ with all other parameters same as in Fig. 3. Results for slow dissipation are shown in thin lines and dissipation by shock waves with power law index $p = 2$ are presented in thick lines. Solid lines are for high magnetic field, $\epsilon_B = 10^{-0.5}$ and dash-dotted lines are for $\epsilon_B = 10^{-6}$. $\epsilon_{pl} = 1$ (thick, solid), and $\epsilon_{pl} = 0$ (thick, dash-dotted).

Ghirlanda, Celloti & Ghisellini 2003; Ryde 2004). As shown in Pe’er, Mészáros & Rees (2005) and as confirmed here (figures 1, 6), for a scattering optical depth larger than ~ 100 , dissipation at a sub-photospheric radius can naturally lead to a clustering of the peak energy at ~ 100 keV – 1 MeV, as observed in many bursts (Brainerd 1998; Preece *et al.* 1998a, 2000).

For low values of the optical depth, $\tau_{\gamma e} \sim 0.1 - 1$, the advected thermal component produces an observed peak at a few tens of keV. This peak energy is consistent with the peak energy observed in X-ray flashes at ~ 25 keV (Heise *et al.* 2001) and X-ray-rich GRB’s (XRR’s), which show peak energy clustering at ~ 50 keV (Sakamoto *et al.* 2005). Thermal peak energies in this range of few tens of keV are obtained for a wide range of values of the free model parameters, $10^{-4} \lesssim L_{52} \lesssim 1$, $1 \lesssim \Gamma_2 \lesssim 3$ and $1 \lesssim \alpha \lesssim 10^3$ which result in an op-

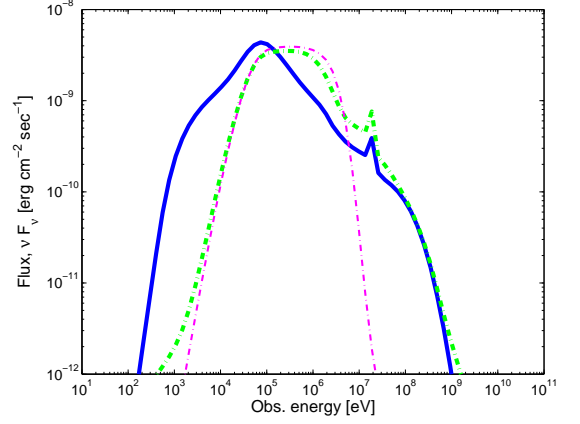


FIG. 5.— Time averaged spectra obtained for intermediate value of the optical depth, $\tau_{\gamma e} = 10$. Results are shown for $L = 10^{-1}$ with all other parameters same as in Fig. 3. Results for slow dissipation are shown in thin lines and dissipation by shock waves with power law index $p = 2$ are presented in thick lines. Thick, solid line: high magnetic field, $\epsilon_B = 10^{-0.5}$ and $\epsilon_{pl} = 0$. Thick, dash-dotted line: $\epsilon_B = 10^{-4}$, $\epsilon_{pl} = 1$. Thin, dash-dotted: slow heating, $\epsilon_B = 10^{-6}$.

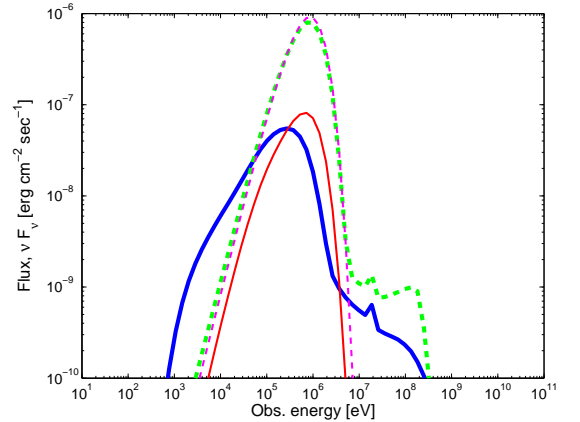


FIG. 6.— Time averaged spectra obtained for high value of the optical depth, $\tau_{\gamma e} = 100, 1000$. Results are shown for $L = 1$ (solid), $L = 10$ (dash-dash) with all other parameters same as in Fig. 3. Results for slow dissipation are shown in thin lines and dissipation by shock waves with power law index $p = 2$ are presented in thick lines. Thick, solid line: high magnetic field, $\epsilon_B = 10^{-0.5}$ and $\epsilon_{pl} = 1$. Thick, dash-dash line: $\epsilon_B = 10^{-6}$, $\epsilon_{pl} = 0.1$. Thin, solid: slow heating, $\epsilon_B = 10^{-0.5}$. Thin, dash-dash: slow heating, $\epsilon_B = 10^{-6}$.

tical depth ~ 1 (see eqs.1,2). It is difficult to obtain in our model a thermal peak energy at energies below a few keV combined with an optical depth larger than $\sim 10^3$. Therefore, for a peak below a few keV, electrons maintain their energy (see §4). We conclude that if XRF’s peak energies are due to advected thermal component, no XRF’s with peak energy below a few keV are expected.

The inclusion of an advected thermal component in the prompt emission calculations can help resolving the question of the accelerated electron distribution, which is of high theoretical importance. As pointed out by Baring & Braby (2004), fitting the data of many GRB’s by synchrotron and Compton emission only, require the acceleration of the majority of electrons to a power law distribution, leaving far too few thermal particles than

to be expected as a seed distribution for the power law population. Here, we overcome this problem by assuming that the thermal component seen in many bursts (e.g., Ryde 2004), and presumably exist in all of them at early times, is advected from the core. As a result, a variety of spectra can be obtained under different assumptions on the values of the free parameters, without the requirement that most of the electrons are accelerated to a power law distribution (in the presented figures of the power law acceleration model, we allow the parameter ϵ_{pl} to vary between 0 and 1).

The spectra presented in this paper (§5) describe the emission resulting from a single dissipation phase (e.g., single collision between two shells) for a particular choice of model parameters. Observed spectra are expected to be combination of spectra produced by many such dissipation processes, which are characterized by different parameters, e.g., different locations of collisions within the expanding wind. A detailed comparison with observations therefore requires a detailed model describing the distribution of single dissipation parameters within the fireball wind (see, e.g., Daigne & Mochkovitch 1998; Panaitescu, Spada & Mészáros 1999; Guetta, Spada & Waxman 2001). The construction and investigation of such detailed models would involve additional assumptions and parameters, which is beyond the scope of this manuscript.

Nonetheless, the similarities found between the resulting spectra, produced under reasonable assumptions about the unknown values of the free parameters, suggests that the key results would remain valid for a spectrum that is obtained from a series of dissipation processes. These results include an observed break energy at few tens of keV to sub MeV, accompanied by slopes steeper than the optically thin synchrotron spectrum at lower energies, which are obtained for a single dissipation event for any value of the optical depth, and flat energy per decade spectra obtained up to sub-GeV energy for optical depths of 10^{-2} - few tens. For a superposition of dissipation events at various radii, flatter slopes can be obtained.

A superposition of dissipation events is also required

in our model in order to explain both peak clustering at ~ 300 keV and flat energy per decade spectra at higher energies, as observed in many GRB's. A high optical depth $\tau_{\gamma e} \gtrsim 100$ is required in order to obtain a Wien peak at sub-MeV energies, while lower values of $\tau_{\gamma e}$ are required in order to obtain a flat energy per decade spectra at higher energies. As detailed in (Pe'er & Waxman 2004; Pe'er, Mészáros & Rees 2005), for the case of high optical depths the photons are expected to lose $\sim 30\%$ of their energy to the bulk motion of the plasma during an adiabatic expansion phase before escaping, thus the observed Wien peak energy is expected at ~ 300 keV. We conclude that given such a superposition, a clustering of the peak energy, steep slopes below the peak and flat energy per decade spectra above the break are a natural consequence of a model containing a significant thermal emission component. These results show good agreement with a large number of observations of GRB prompt emission spectra (Band *et al.* 1993; Preece *et al.* 2000; Ryde 2004).

The fluxes predicted by the model are within the detection capability of the Swift⁴ satellite in the keV range, and the GLAST⁵ satellite in the sub- GeV range. Observations of a cutoff at high energies will therefore provide information about the optical depth during the dissipation phase, hence constraining the value of Γ , one of the least constrained free parameters of the model.

The results may be applicable to a variety of compact objects, such as GRB's, XRF's and blazars. At least 60 flat spectrum radio quasars having flat ($\alpha \approx 0$) spectral index in the EGRET range were reported (e.g., Mukherjee *et al.* 1997). Similar spectra were obtained for several quasars using the BeppoSAX satellite (Tavecchio 2000), while clustering of blazars peak energies at 1-5 MeV was reported by McNaron-Brown *et al.* (1995). We thus conclude that similar mechanisms to the ones presented here may explain some of the observable effects in radio quasars as well.

AP wishes to thank R.A.M.J. Wijers for useful discussions.

⁴ <http://www.swift.psu.edu>

⁵ <http://www-glast.stanford.edu>

APPENDIX

ENERGY LOSS RATE OF HIGH ENERGY PHOTONS DUE TO COMPTON SCATTERING WITH MILDLY RELATIVISTIC ELECTRONS

The rate of scattering by a single electron having Lorentz factor γ passing through space filled with a unit density, isotropically distributed, mono-energetic photons with energy $\alpha_1 m_e c^2$ was first derived by Jones (1968), and summarized in Pe'er & Waxman (2004b),

$$\frac{d^2 N(\gamma, \alpha_1)}{dt d\alpha} = \frac{\pi r_0^2 c \alpha}{2\gamma^4 \beta \alpha_1^2} [F(\zeta_+) - F(\zeta_-)]. \quad (\text{A1})$$

Here, α is the energy of the outgoing photon in units of $m_e c^2$, r_0 is the classical electron radius, $\beta = (1 - 1/\gamma^2)^{1/2}$, ζ_{\pm} are the upper and lower integration limits and $F(\zeta)$ is given by the sum of 12 functions, $F(\zeta) = \sum_{i=1}^{12} f_i(\zeta)$, where the functions $f_i(\zeta)$ are summarized in, e.g., eq. 20 of Pe'er & Waxman (2004b).

The limits $\zeta_{\pm}(\alpha; \gamma, \alpha_1)$ depend on the energy of the outgoing photon, α for given α_1 and γ (see Pe'er & Waxman 2004b). For $\alpha_1 \gg 1$ and $\gamma \simeq 1$, this dependence is degenerated and $\zeta_{\pm} = 1 \pm \beta$. In this approximation, in calculating the difference of the 12 function $\Delta f_i \equiv f_i(\zeta_+) - f_i(\zeta_-)$ only 4 out of the 12 terms are to the order α_1^{-1} or α^{-1} , while

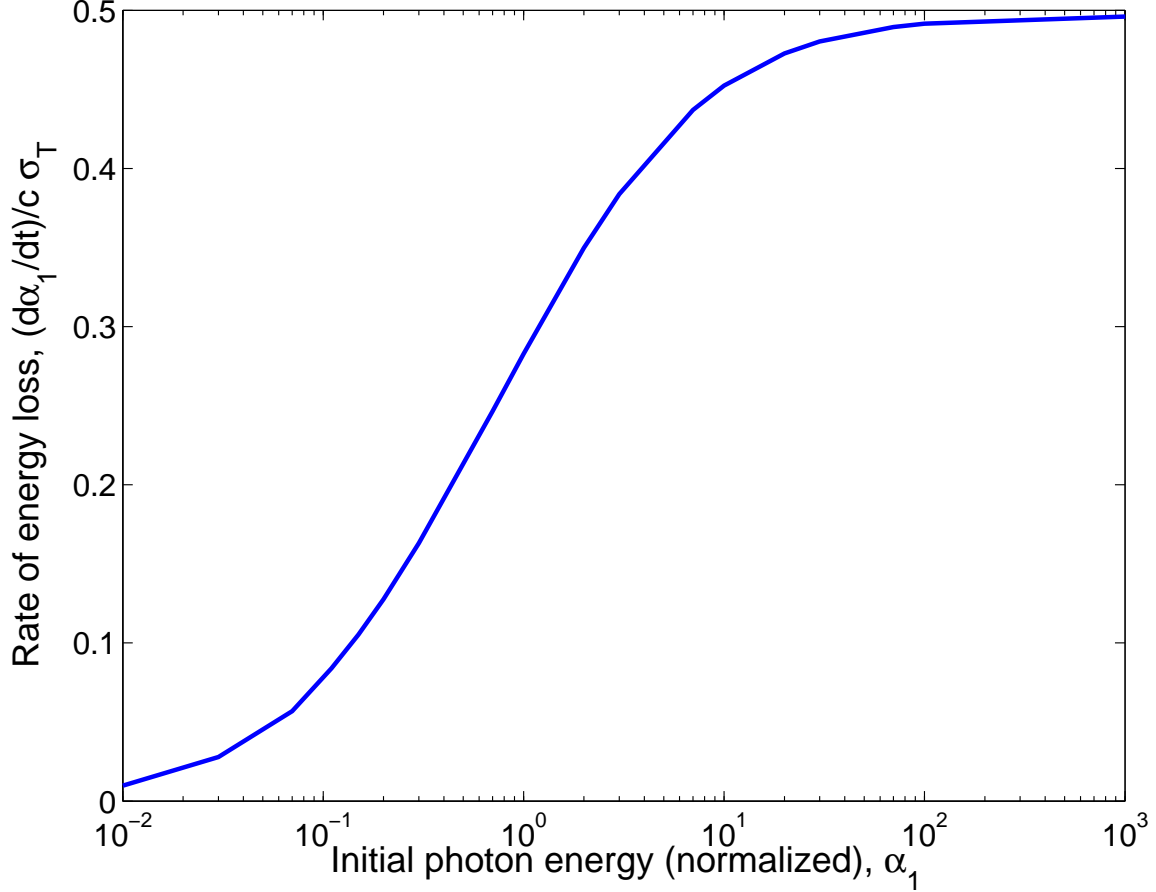


FIG. A7.— Energy loss rate of photon with initial energy $\alpha_1 m_e c^2$ due to Compton scattering with unit density, isotropically distributed, mono-energetic electrons with velocity $\beta = 0.1$.

the other 8 are to lower orders in α , α_1 . Thus, to leading order in α , α_1 ,

$$\begin{aligned} \Delta f_3 &\equiv f_3(\zeta_+) - f_3(\zeta_-) \simeq \frac{2\beta}{(1-\beta^2)\alpha_1}, \\ \Delta f_9 &\simeq \frac{2\beta(1+\beta^2)}{\alpha}, \\ \Delta f_{10} &\simeq \frac{\beta^3}{\alpha}, \\ \Delta f_{11} &\simeq \frac{2\beta(1+\beta^2)}{\alpha^2} \left[\alpha_1 - \alpha + \left(1 + \frac{\alpha_1}{\alpha}\right) \left(1 + \frac{\beta^2}{2}\right) \right]. \end{aligned} \quad (\text{A2})$$

The (normalized) energy loss rate of photon being scattered by unit density, isotropically distributed, mono-energetic electrons at Lorentz factor γ is therefore given by

$$\frac{d\alpha(\gamma, \alpha_1)}{dt} = \int_{\alpha_{min}}^{\alpha_1} \alpha' \frac{d^2 N(\gamma, \alpha_1)}{dt d\alpha'} d\alpha' \simeq c\sigma_T \left(\frac{1-\beta^2}{2} + \frac{3\beta^2}{16} \right) = c\sigma_T \left(\frac{1}{2} - \frac{5\beta^2}{16} \right) + O(\alpha_1^{-1}). \quad (\text{A3})$$

In order to check the validity of this approximation for values of α_1 not much larger than 1, a numerical integration of equation A1 was carried out, using the exact formula. The results of the energy loss rate are presented in Figure A7. From the figure we find that the approximation $d\varepsilon/dt \approx c\sigma_T m_e c^2/2$, where $\varepsilon = \alpha m_e c^2$ for the energy loss rate of photon due to Compton scattering with unit density, isotropically distributed, mono-energetic electrons with $\gamma \approx 1$ is valid for $\varepsilon \geq f m_e c^2$, with $f \approx 3$.

REFERENCES

- Band, D., *et al.* 1993, ApJ, 413, 281
 Baring, M.G., & Braby, M.L. 2004, ApJ, 613, 460
 Brainerd, J.J. 1998, in the 19th Texas Symposium on Relativistic Astrophysics and Cosmology, Eds.: J. Paul, T. Montmerle, and E. Aubourg (Paris: CEA Saclay)
 Crider, A., *et al.* 1997, ApJ, 479, L39
 Daigne, F., & Mochkovitch, R. 1998, MNRAS, 296, 275
 Frontera, F., *et al.* 2000, ApJS, 127, 59
 Ghirlanda, G., Celotti, A., & Ghisellini, G. 2003, A&A, 406, 879
 Ghisellini, G., & Celotti, A. 1999, ApJ, 511, L93
 Giannios, D., & Spruit, H. 2005, A&A, 430, 1
 Guetta, D., Spada, M., & Waxman, E. 2001, ApJ, 557, 399
 Heise, J. in't Zand, J., Kippen, R.M., & Woods, P.M. 2001, in Gamma-Ray Bursts in the Afterglow Era, ed. E. Costa, F. Frontera, & J. Hjorth (Berlin: Springer), 16
 Jones, F.C. 1968, Physical Review, 167, 1159

- Liang, E. P., Kusunose, M., Smith, I., & Crider, A. 1997, *ApJ*, 479, L35
- Liang, E. P. 1997, *ApJ*, 491, L15
- McNaron-Brown, K., *et al.* 1995, *ApJ*, 451, 575
- Mukherjee, R., *et al.* 1997, *ApJ*, 490, 116
- Mészáros, P. 2002, *ARA&A*, 40, 137
- Mészáros, P., Ramirez-Ruiz, E., Rees, M.J., & Zhang, B. 2002, *ApJ*, 578, 812
- Mészáros, P., & Rees, M.J. 2000, *ApJ*, 530, 292
- Panaitescu, A., Spada, M., & Mészáros, P. 1999, *ApJ*, 522, L105
- Pe'er, A., Mészáros, P., & Rees, M.J. 2005, *ApJ*, in press (astro-ph/0504346)
- Pe'er, A., & Waxman, E. 2004, *ApJ*, 613, 448
- Pe'er, A., & Waxman, E. 2004, *ApJ*, 628, 857
- Piran, T. 2004, *Rev. Mod. Phys.* 76, 1143
- Pozdniakov, L.A., Sobol, I.M., & Sunyaev, R.A. 1983, *ASPRv2*, 189
- Preece, R., *et al.* 1998, *ApJ*, 496, 849
- Preece, R., *et al.* 1998, *ApJ*, 506, L23
- Preece, R., *et al.* 2000, *ApJs.s.*, 126, 19
- Preece, R., *et al.* 2002, *ApJ*, 581, 1248
- Ramirez-Ruiz, E. 2005, *MNRAS*, in press (astro-ph/0509232)
- Rees, M.J., & Mészáros, P. 1994, *ApJ*, 430, L93
- Rees, M.J., & Mészáros, P. 2005, *ApJ*, 628, 847
- Ryde, F. 2004, *ApJ*, 614, 827
- Sakamoto, T., *et al.* 2005, *ApJ*, 629, 311
- Sari, R., & Piran, T. 1997, *ApJ*, 485, 270
- Sunyaev, R.A., & Titarchuk, L.G. 1980, *A&A*, 86, 121
- Tavani, M. 1996, *ApJ*, 466, 768
- Tavecchi, F. *et al.* 2000, *ApJ*, 543, 535
- Thompson, C. 1994, *MNRAS*, 270, 480
- Waxman, E. 2003, *Gamma-Ray Bursts: The Underlying Model, in Supernovae and Gamma-Ray bursters*, Ed. K. Weiler (Springer), *Lecture Notes in Physics* 598, 393–418.
- Woods, E., & Loeb, A. 1995, *ApJ*, 453, 583
- Zdziarski, A.Z. 1986, *ApJ*, 303, 94
- Zdziarski, A.Z., *et al.* 1994, *MNRAS*, 269, L55